A trait-based carbon export model for mesopelagic fishes in the Gulf of Mexico with consideration of asynchronous vertical migration, flux boundaries, and feeding guilds

Authors: Matthew S. Woodstock[*1], Tracey T. Sutton[2], Yuying Zhang[1]

Affiliations: [1]Department of Biological Sciences, Oceans and Coastal Division, Institute of Environment, Florida International University, 3000 NE 151st St. North Miami, FL

[2]Department of Marine and Environmental Sciences, Nova Southeastern University, 8000 N. Ocean Dr., Dania Beach, FL

Corresponding Author: Matthew S. Woodstock; mwood078@fiu.edu

Co-Author Emails: Tracey T. Sutton: tsutton1@nova.edu; Yuying Zhang: yzhang13@fiu.edu

Abstract

Fish-mediated carbon export provides a significant proportion of the biological carbon pump in oligotrophic regions. Bioenergetic models estimate this carbon transport, but many lack species-specific traits and no carbon export model has been developed in the mesopelagic Gulf of Mexico. Intensive mesopelagic sampling efforts in the northern and eastern Gulf of Mexico have provided high-resolution information regarding community composition, species' vertical migratory characteristics, diel depth occupancies, and diets. A stochastic, individual-based model was developed for deep-pelagic fishes in the northern Gulf of Mexico to estimate bioenergetic rates and carbon export fluxes. Fishes that ate gelatinous zooplankton consumed more mass per body weight per day than predators of cephalopods and fishes, ostensibly to increase the throughput of prey with less carbon (gelata) or more refractory materials (Crustacea). A dynamic energy budget submodel indicated that during 81% of occurrences, asynchronous vertically migrating fishes rested for one day before migrating again, but migrations on successive days

were possible. In terms of carbon export, myctophids and stomiids contributed greater than 53% and 12% of the active carbon flux for the entire assemblage in all scenarios. The assemblage-wide carbon export rate driven by vertically migrating fishes was 0.14–0.72 mg C m^{-2} d^{-1}, 61% of the ingested carbon by the assemblage. Incorporating species-specific traits and individual variability in bioenergetic models allows for more complex research questions (e.g., the effect of feeding guilds and asynchronous migration on carbon export) compared to the carbon export models that otherwise assume all fishes within a functional group are equivalent.

Keywords

Bioenergetic Modeling; Carbon export; Diel Vertical Migration; Gulf of Mexico; Mesopelagic; Myctophidae; Trait-based Model

Introduction

The increase in anthropogenic CO_2 in the atmosphere and its effect on the environment have prompted urgent interest in the global carbon cycle. Carbon is actively transported in the deep sea by vertically migrating organisms, namely zooplankton, pelagic shrimps, fishes, and cephalopods (Ducklow et al. 2001; Lomas et al. 2010; Judkins 2014). More specifically, fishes contribute to active carbon flux by respiring CO_2, defecating fecal pellets, excreting calcium carbonate, sinking upon mortality, and being consumed in the deep sea (Radchenko 2007; Wilson et al. 2009). The fish biomass in the mesopelagic zone (200–1000 m depth) has been estimated from 1.8–16 Gt, dominating the global fish biomass and suggesting that they are an integral contributor to the sequestration of carbon into the deep sea (Irigoien et al. 2014; Proud et al. 2019). Estimations of fish-mediated carbon export are typically developed through bioenergetic models, but these models often lack species-specific traits that likely influence carbon flux estimates.

47 Bioenergetic models are based on quantitative rate processes of fishes and the abundance of
48 each trophic guild within fish assemblages. Calculating biological rates (e.g., metabolism,
49 respiration) for deep-pelagic fishes in the field is untenable due to the difficulty of obtaining
50 unstressed, living individuals from field surveys. Therefore, bioenergetic rate estimates for deep-
51 sea fishes are derived from the metabolic theory of ecology, which is a function of temperature,
52 animal mass, and depth (Gillooly et al. 2001; Ikeda 2016). Reduced metabolism at depth has also
53 been hypothesized to result from a logarithmic decline of food energy available at increasing
54 depth (Haedrich 1996) and the preponderance of gelatinous zooplankton in the deep pelagial
55 (Sutton 2013), which results in an alternative trophic pathway in oceanic ecosystems (Haddock
56 2004; Choy et al. 2017). From the metabolic rate estimate, ingestion and respiration rates can
57 also be estimated (Brett and Groves 1979; Davison et al. 2013). Laboratory techniques have been
58 used to estimate the activity of the electron transport chain as a proxy for respirometry (Childress
59 and Somero 1979; Gibbs and Somero 1989), but these methods do not always agree with
60 regression-based estimates (Hernández-León et al. 2019a). Fishes excrete carbon through two
61 pathways, either as dissolved organic carbon through gut fluids or inorganic calcium carbonate
62 excretion through the alimentary canal. These excretion rates can be estimated as a function of
63 temperature and animal mass (Wilson et al. 2009). Defecation rates are ideally calculated as a
64 function of the digestion rate of the prey and the gut evacuation rate of the predator. Gut
65 evacuation rates for mesopelagic fishes range between 2 and 10 hours (Clarke 1978; Pakhomov
66 et al. 1996; Hudson et al. 2014), but digestion rates are unknown. Instead, defecation rates can be
67 estimated as a function of ingestion rates and the proximate composition of the preys (Davison et
68 al. 2013). Although limited to empirical estimates of bioenergetic rates, introducing species-
69 specific diets, depth distributions, and diel vertical migratory behaviors into carbon export

models should provide fish-mediated carbon flux estimates with consideration to the diverse life histories of mesopelagic fishes.

Diel vertical migration is often considered a binary trait, where species are classified as synchronous vertical migrators (migrate each day) or non-migrators. However, several core assemblage members are classified as asynchronous vertical migrators, where only a portion of the population migrates each night (Gartner Jr et al. 1987). While these fishes are not migrating, they are believed to be "fasting" until they need to consume their next meal (Sutton and Hopkins 1996). Foraging decisions can be incorporated into dynamic energy budget models as a probabilistic function where the amount of energy in reserve dictates the probability of an animal deciding to forage (Kooijman 2010). In asynchronous migrating organisms, stored lipid concentrations sharply increase in response to feeding events and gradually decline with maintenance costs (e.g., metabolism; Pearre 2003), indicating that lipid concentrations are a suitable proxy to control the probability of foraging, and associated vertical migration, by asynchronous vertical migrators. The periodicity at which a fish migrates is expected to influence the carbon the fish actively transports.

The depth at which carbon is considered "exported" into the deep sea may influence the carbon export model output when considering species-specific depth distributions and migratory behavior. In models, flux boundaries are typically set at the shallowest depth sampled via sediment traps, but the actual depth of a flux boundary is likely a function of dynamic oceanographic characteristics (Buesseler et al. 2020). The flux boundary may also be disparate for different energetic processes, as waste products have varying densities that result in different sinking velocities (Yoon et al. 2001). In carbon export models, flux boundary depths are

92 generally between 100–200 m, but a direct comparison of flux boundary variation is lacking
93 (Saba et al. 2021).

94 Carbon export models utilize empirical relationships and physiological rates in concert with
95 fish biomass estimates to quantify carbon transfer through fish feeding. The accuracy of these
96 models relies on the accuracy of the data and relationships that are used to build them.
97 Physiological rates can vary by a factor of *c.* 2 (Q10 Rule; Eppley 1972), while biomass
98 estimates may vary by orders of magnitude on small scales (e.g., 10 m; Angel 1993). Therefore,
99 the accuracy of carbon export models is more reliant on biomass estimates than physiological
100 rate estimates. Between 2011 and 2021, two sampling programs, ONSAP and DEEPEND
101 (www.deependconsortium.org), have quantitatively sampled and developed a time series of
102 discrete-depth fish abundances in the mesopelagic Gulf of Mexico (Cook et al. 2020; Sutton et
103 al. 2020), resulting in perhaps the largest deep-pelagic fish collection of its kind in
104 oceanographic history. These unparalleled community data allow for the construction of more
105 comprehensive bioenergetic and carbon export models than previously possible.

106 *Objectives*

107 In this study, we developed a trait-based model that estimates fish energetic rates (i.e.,
108 defecation, excretion, metabolism, ration, respiration) according to empirical relationships.
109 Fishes were assigned to feeding guilds and then compared to determine if the interplay between
110 prey quality and feeding rate influences carbon flux. Species-specific, size-based regressions
111 were performed to investigate the change in feeding rate as a function of fish size. An important
112 differentiation was made during the modeling process between synchronous vertical migrators,
113 asynchronous vertical migrators, and non-migrators to increase the precision of carbon flux
114 estimation and determine how energy storage affects the vertical migration periodicity of

asynchronous migrators (days between feeding intervals). Finally, the amount of carbon transported across multiple flux boundaries was determined to identify the key species in carbon transposition, and this amount was elevated to the assemblage scale to provide an assemblage-based carbon export estimate for mesopelagic fishes in the northern and eastern Gulf of Mexico.

Methods

Sample collection

Micronekton were collected from 2011–2018 on various cruises aboard the research vessels *Meg Skansi* and *Point Sur* in the oceanic Gulf of Mexico (Cook et al. 2020). This sampling primarily occurred seaward of the 1000-m isobath within a spatial grid bound by -90W, -84W, 26N, and 30N (Figure 1), which is used as the model domain. The main gear type of these surveys was a 10-m^2 Multiple Opening and Closing Environmental Sensing System (MOCNESS) that sampled discrete depth intervals from the surface to 1500 m. This model restricts those data to the top 1000 m of the water column (epipelagic and mesopelagic zones) and only considers "Gulf Common Water" sampling stations (*sensu* Johnston et al. 2019). From this subset, the relative abundance that each species contributes to the micronekton fish assemblage was calculated. Prior to fixation, each fish was measured to the nearest 1 mm standard length. All biological data are publicly available through the GRIIDC data repository (https://data.gulfresearchinitiative.org/).

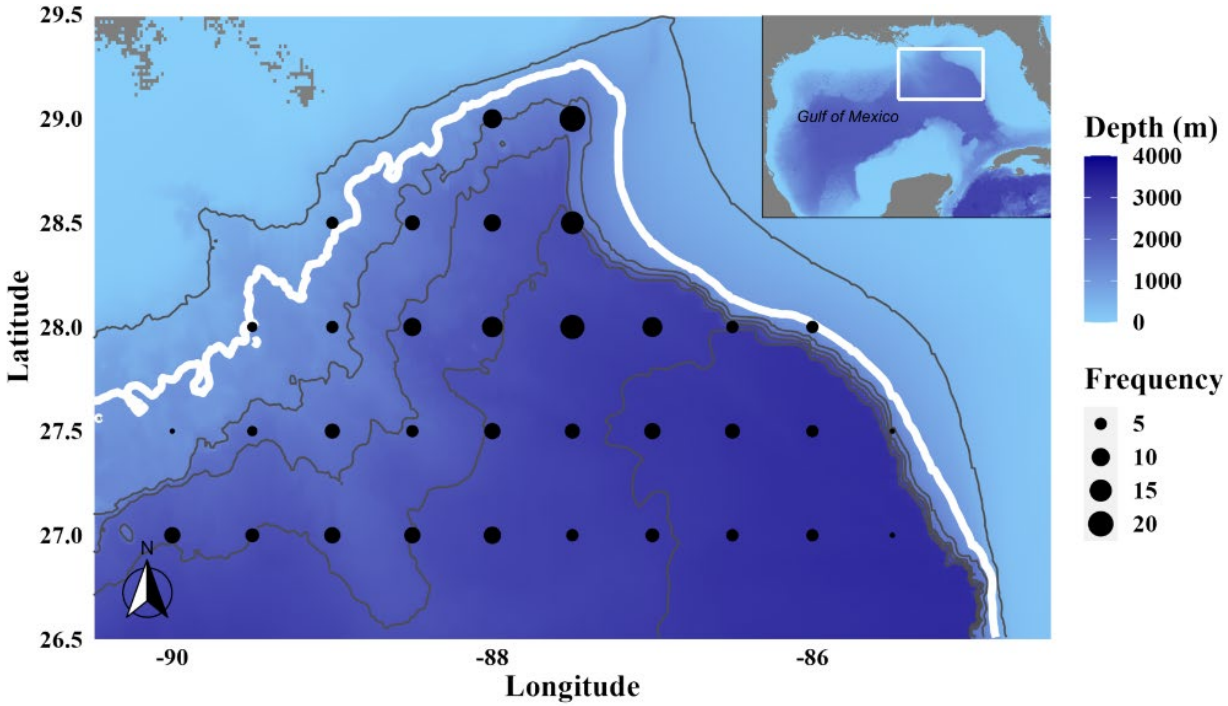

Figure 1. Map of the model domain. The model is bounded inshore by the 1000 m isobath (white line). Trawl locations are denoted as black circles, sized to deployment frequency. Other isobaths are denoted as black lines representing the 500, 1,500, 2,000, 2,500, and 3,000 m isobaths moving seaward. Bathymetry data were queried from the R "marmap" package.

Temperature data

Temperature data were collected from the HYCOM hourly dataset GOM10.04 (www.hycom.org). This dataset includes 26 depth intervals in the top 1000 m, with a horizontal spatial resolution of 1/25°. Data were gathered from January 1st, 2015, to December 31st, 2018. Hourly temperature averages were calculated as the geometric mean for each node on the 3-dimensional grid from the four years. Daily daytime and nighttime temperatures were calculated from the hourly temperatures as the geometric mean of the hours between 0700 and 1900 (local daytime) and 2000 to 0600 (local nighttime). These temperatures were applied to individuals in the model (Figure 2).

148 *Model description*

149 A trait-based model was developed that incorporates species-specific differences at an
150 individual scale (Figure 2). Individual fishes were simulated from January 1st to December 31st
151 on a diel time interval (day and night; 12-hour time steps). At each time step, fishes undergo
152 processes of vertical migration, ingestion, respiration, carbonate excretion, defecation, and
153 mortality. For each iteration, the species and all associated traits were assigned according to the
154 relative abundance from field surveys (i.e., a species that contributed 5% of the total number of
155 fishes caught had a 5% chance of being selected in each iteration). This process weights all
156 results by the relative abundance in the net-caught assemblage (Figure S1). Leptocephali (i.e.,
157 anguilliform eel larvae) were excluded from the model because they allocate most of their
158 ingested energy into metabolism (>60%), while non-leptocephalus larvae allocate more energy
159 towards growth (Bishop and Torres 2001). Length-frequency distributions for species that
160 amounted to greater than 25 individuals during sampling were fit to lognormal distributions to
161 which the length of the modeled individual was chosen randomly (Figure 2). Since random
162 selection from a lognormal distribution has a small probability of selecting an unrealistically
163 high value, the maximum length of a species was capped at 5% greater than the largest fish
164 captured during sampling. For species that amounted to less than 25 individuals, the length was
165 randomly selected between the minimum and maximum lengths captured. Length-weight
166 regressions were gathered from literature sources and used to estimate weight from length. This
167 model utilizes dry weights, so if only a length-wet weight regression was available for a species,
168 a mass conversion factor was applied according to the proximate composition of mesopelagic
169 fishes in the eastern Gulf of Mexico (Stickney and Torres 1989). Species that were missing life
170 history information were assigned parameters from closely related species.

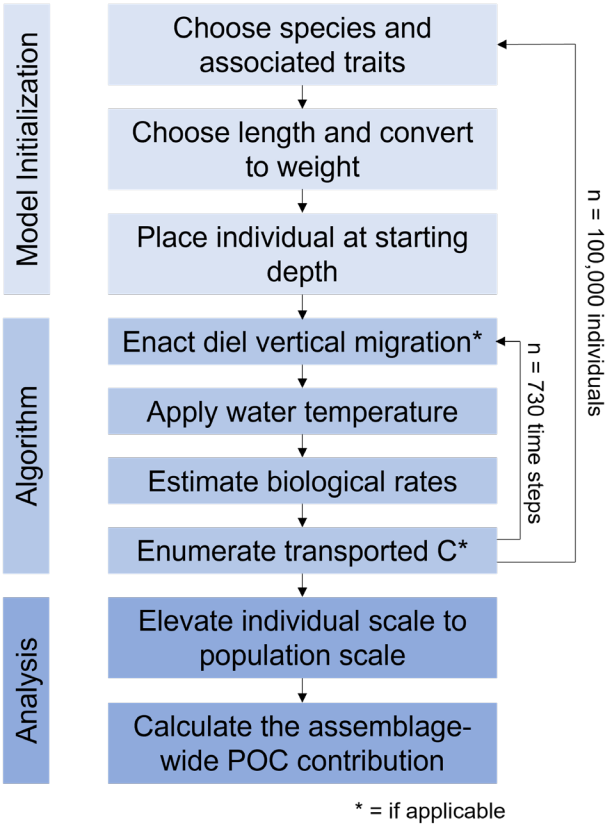

Figure 2. A flow chart showing the model process for each scenario. For each individual, the algorithm looped 730 times to simulate day and night for 365 calendar days. One hundred thousand individuals were run for each scenario.

The type of diel vertical migration behavior and depth ranges (both daytime and nighttime) were gathered from literature and survey data. The depth of an individual at a particular time step was a random value between the minimum and maximum depth for that species and the diel period (Table S2). The individual was placed at a random latitude and longitude within the domain boundaries to incorporate the potential effect of environmental spatial heterogeneity within the northern Gulf of Mexico.

The simulation started after the individual was characterized and assigned a location within the 3-dimensional grid (Figure 2). Vertical migration occurred at the beginning of each time step, but the migration decision of asynchronous vertical migrators (i.e., decision to migrate that night or not) was driven by a dynamic energy budget submodel that estimated the fish's storage energy

(Supplemental Material; Kooijman 2010; Jusup et al. 2011). In this submodel, the fish's reserve energy was increased during feeding events and decreased at all time steps to cover metabolic costs. A lesser amount of stored energy equated to a greater probability that fish would migrate during that time step, and a large amount of stored energy (e.g., the fish ate the night before) resulted in a nearly zero chance the fish would migrate, which aligns with the hunger-satiation hypothesis (Pearre 2003; Bos et al. 2021). A temperature value was applied to the fish according to the latitude, longitude, depth, diel period, and day of the year using a trilinear interpolation method that calculates a weighted average according to the fish's location within a grid cell (Johnston and Bernard 2017). All equations and parameters were described in the Supplemental Material. The resting metabolic rate (RMR; $\mu l\ O_2\ h^{-1}$; Ikeda 2016) was estimated as a function of body mass, temperature, and depth. RMR was converted into KJ h^{-1} using a conversion into g O_2 l^{-1} of 1.43 (Gillooly et al. 2001) and an oxycalorific coefficient of 13.6 KJ g^{-1} (Brett and Groves 1979). The active metabolic rate (*AMR;* migration and feeding) and standard metabolic rate (*SMR;* non-feeding) were calculated as the *RMR* multiplied by a factor of 4 and 0.5 respectively (Winberg 1956; Brett and Groves 1979).

For vertically migrating fishes, a predation success rate of 90% (i.e., the fish had a 90% chance of feeding) was utilized at night to incorporate the possibility of predation failure. A daytime predation success rate was set at 5% because of the possibility that fishes feed at depth (Pearcy et al. 1979). Given that fishes undergo vertical migration to enhance predation success, it was assumed unlikely that daytime feeding is as intense as nighttime feeding. Asynchronous migrating fishes that did not migrate had a 5% chance of predation regardless of the diel period. Non-migrating fishes had a 90% chance of feeding during each stage of the diel period but were restricted to one meal in a 24-hour period. If the fish fed, an ingestion rate (KJ $timestep^{-1}$) was

208 calculated as the product of metabolic rate (*MR*), and an ingestion coefficient specific to vertical
209 migration habit. The *MR* applied depended on the activity of the individual during that time step.
210 Vertically migrating fishes spent four hours migrating at dawn and dusk, cumulatively (Bianchi
211 and Mislan 2016).

212 Carbon was only considered "exported" if first consumed above a flux boundary (default =
213 150 m) and then moved deeper. A daily feeding ration (mg C d^{-1}) was calculated as the quotient
214 of the ingestion rate and the caloric value of prey. Each species had a proportional prey diet
215 according to literature values (Table S3). Juvenile conspecifics of epipelagic fishes were
216 assumed to have a diet consisting of either crustaceans or fishes. To include the influence of
217 different fish feeding guilds (>50% prey weight), prey quality was a function of the proximate
218 composition of preys. The percent bodyweight consumed per feeding interval was calculated as
219 the quotient of the biomass consumed per feeding interval and fish weight. Carbon respiration
220 (mg C $timestep^{-1}$) was estimated using a respiratory quotient (0.9), oxycalorific coefficient, and
221 *MR*. Carbon defecated above the flux boundary is passively exported into the deep via fast-
222 sinking rates (Robison and Bailey 1981), while defecation below the flux boundary has been
223 actively transported, but these are treated as one entity in this model. Defecated carbon (mg C
224 day^{-1}) was a function of feeding ration, digestion efficiencies, and conversions of
225 macromolecules to both prey weight and carbon. Macromolecule to carbon conversions were
226 derived from the proximate composition of the prey taxa and digestion efficiencies (Brett and
227 Groves 1979). Carbon excreted as calcium carbonate (mg C $timestep^{-1}$) was estimated as a
228 function of body mass and temperature (Wilson et al. 2009).

229 Exported carbon associated with fish mortality below the flux boundary (mg C d^{-1}) is the
230 function of a growth function, carbon-dry weight conversion of the fish, and specific energy

content of fish. Growth was calculated as the product of the ingestion rate and 0.16 (Davison et al. 2013). Fish mortality (*M*) was a stochastic procedure where the daily probability of *M* occurring was estimated as the proportion of total mortality not derived from epipelagic predators in an ecosystem model for the region (derived from Woodstock et al. 2021). The values for *M* were 0.143, 0.227, 0.378, 0.0925, 0.15, and 0.427 for gonostomatids, myctophids, sternoptychids, stomiids, other mesopelagic micronektonivores (cephalopod and fish feeding guilds), and other mesopelagic zooplanktivores, respectively.

The daily carbon export for a fish is the sum of carbon exported via defecation, excretion, respiration, and mortality processes. A vertically integrated abundance (n m^{-2}) was calculated from trawl data for each species from 2015–2018, and a 14% capture efficiency was used and applied to the abundance estimates (Koslow et al. 1997). Prior sampling years were excluded from the abundance calculation because of a noted population decline of many mesopelagic fish taxa (Sutton et al. submitted). The daily carbon export was multiplied by the species' abundance to create a population-scale carbon export estimate (mg C m^{-2} d^{-1}). Assemblage-wide particulate organic carbon (POC) estimates were calculated as the sum of all population contributions. A daily POC estimate for the model domain was obtained from the Copernicus Marine Environment Monitoring Service (CMEMS; http://marine.copernicus.eu/; Sauzède et al. 2020). The assemblage POC was divided by the particulate organic carbon estimate below the flux boundary to calculate the %POC derived from mesopelagic fishes. Although excretory carbon (calcium carbonate) and respiratory carbon (CO_2) produce different compounds, these were still calculated in relation to water column POC for comparative purposes.

The model was run under three scenarios to explore the effect different flux boundaries have on carbon export estimates. Each scenario included 100,000 iterations to assure that the modeled

assemblage resembles the sampled micronekton assemblage. Flux boundaries of 100 m, 150 m, and 200 m were examined. Additionally, several parameters were adjusted to calculate the model's sensitivity to temperature, activity rates, ingestion coefficients, respiratory quotient, predation success, prey quality, and fish mortality probability. For the sensitivity analysis, a 30 mm standard length *Lampanyctus alatus* was retained at a depth of 400 m during the day, 50 m depth during the night, and a geographic location of -88ºW and 28ºN to reduce stochasticity. However, mortality and predation success were stochastic processes that could not be ignored, so 1,000 iterations were run for each sensitivity scenario to mitigate the effect of this random process. The total flux contribution was compared to a base model, and the deviations revealed the sensitivity.

Results

Assemblage structure

After 100,000 iterations, the modeled species composition reasonably matched the net-caught species composition, indicating that the modeled assemblage reflects the oceanic Gulf of Mexico micronektonic fish assemblage. The most abundant family, Gonostomatidae, amounted to 60.5% of the relative abundance and 32.7% of the relative biomass (Table 1). The Gonostomatidae was dominated by six species in the genus *Cyclothone,* which alone accounted for 25.1% of the assemblage biomass because of their high relative abundance. Two gonostomatids accounted for greater than 10% of the assemblage biomass each: *Cyclothone pallida* and *Sigmops elongatus*. Myctophids (10.9%), sternoptychids (10.5%), and carangids (3.2%) were the next most abundant families in the model (Table 1). All carangids were larval or juvenile stages of holoepipelagic fishes remaining in the epipelagic zone throughout the day and accounted for 0.4% of the modeled assemblage biomass. Stomiids accounted for 1.7% of the abundance, but their large

277 body sizes represented the fourth greatest biomass proportion of all families (6.7%). The eight
278 most abundant families amounted to 90.8% of the assemblage abundance and 82.7% of the
279 relative weight in the model (Table 1), indicating that this diverse assemblage is dominated by
280 just a few main families.

281

Table 1. The relative abundance and biomass (expressed as %) of modeled individuals organized by family for the families that amounted to greater than 1% of the relative abundance. The proportions of vertical migrators for both family abundance and biomass are listed as well. "-" means no migrators.

Family	Relative Abundance	Proportion Migratory Abundance	Relative Weight	Proportion Migratory Biomass
Gonostomatidae	60.5	2.0	32.7	34.0
Myctophidae	10.9	94.9	27.4	77.0
Sternoptychidae	10.5	16.1	13.2	58.7
Carangidae	3.2	-	0.4	-
Stomiidae	1.7	89.3	6.7	94.4
Melamphaidae	1.5	69.2	1.8	40.4
Phosichthyidae	1.3	98.1	0.5	99.0

Ration

For 61.7% of all modeled species with a sample size greater than 10 (n = 142), larger fishes consumed more carbon per feeding interval than smaller conspecifics (Table S4). Exceptions to this relationship were generally fishes with a narrow size range that did not allow for a broad investigation into size-specific relationships, or a wide depth range that created uncertainty from the metabolic rate equation. All relationships between fish standard length and consumed carbon were best fit to a second-degree polynomial function.

Differences in species' diets and diel vertical migratory behavior influenced the feeding rations of mesopelagic fishes. The percent bodyweight consumed per feeding interval varied among functional groups ($p < 0.001$; Figure 3). The median percent bodyweight consumed of synchronous migrators (3.1% ± 1.3), asynchronous migrators (3.4% ± 1.1), and holoepipelagic non-migrating fishes (4.0% ± 1.9) appear to be consistent. Mesopelagic non-migrating fishes had a lower percent bodyweight consumed (0.9% ± 0.4) than the other functional groups. The percent bodyweight consumed per feeding interval varied according to the feeding guild for all groups ($p < 0.001$). Fishes within the gelatinous zooplankton feeding guild (diet > 50% gelatinous zooplankton) had rations that were factors of 2.2, 1.7, and 2.2 greater than

cephalopod, crustacean, and fish predators in mesopelagic non-migrators, respectively. Among the four most abundant mesopelagic fish families, the percent bodyweight consumed per feeding interval was 1.0% (± 0.4), 3.8% (± 1.3), 1.2% (± 0.8), and 1.8% (± 1.0) bodyweight for the Gonostomatidae, Myctophidae, Sternoptychidae, and Stomiidae, respectively. Within-family variation was caused by the presence of both vertical migrators and non-migrators and species-specific trait differences. Synchronous and asynchronous migrating fishes may consume a similar percent bodyweight per feeding interval, but a greater migration frequency by synchronous migrators indicates these fishes have a greater per capita predation impact on prey communities than asynchronous migrating fishes.

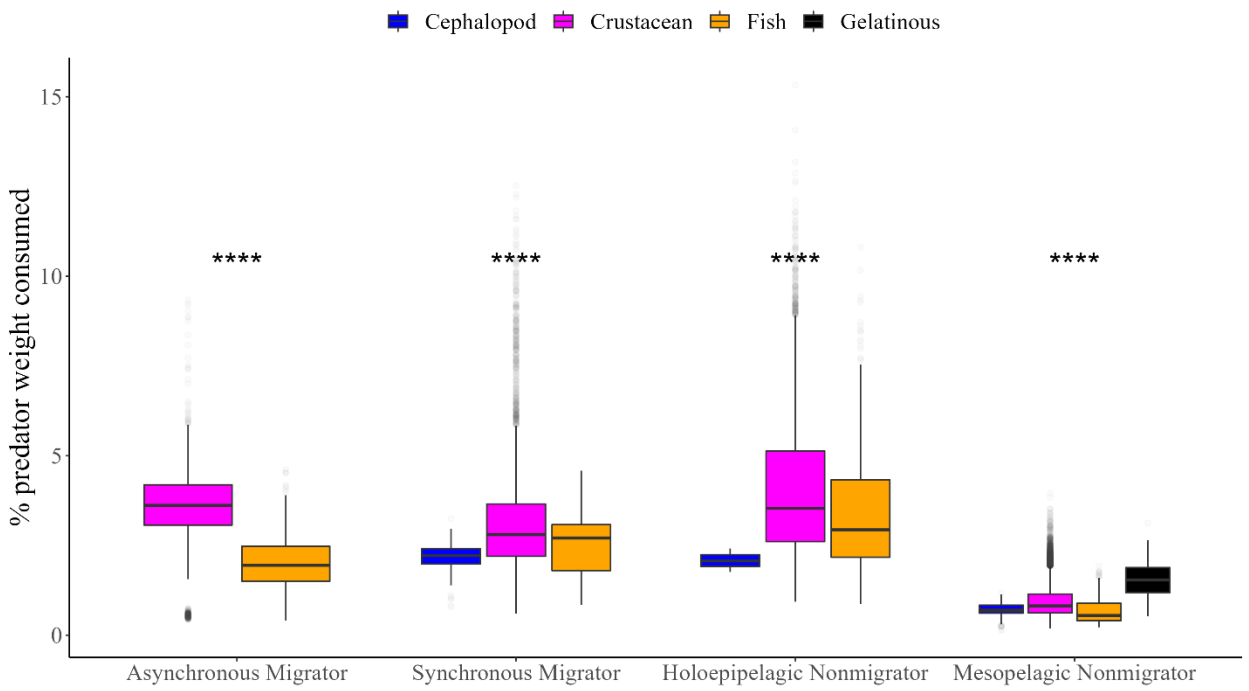

Figure 3. The % bodyweight consumed per feeding interval by functional group and feeding guild. Absent feeding guilds exist when a species does not fit that category. Asterisks represent significance in within-group comparisons.

Asynchronous migration periodicity

Asynchronous vertically migrating fishes rested for one day before migrating again during 81% of potential migrating events (Figure 4). Fishes migrated on successive nights (i.e., zero days off between migrations) during 10% of the possible migrating events. On just one occurrence (8×10^{-5} %), a *Lampadena luminosa* waited seven days before migrating again. There was no difference in asynchronous migration periodicity among species ($p = 0.48$; Figure S2) or within any species, ostensibly because energy assimilation and usage are a function of body size. The consumption of larger prey items (i.e., higher ration) did not significantly increase the wait time between migration ($p = 0.5$). Although counterintuitive, this model does not incorporate satiation by individuals that consume more than the amount required for their energetic demand. Therefore, the asynchronous migration periodicity for this model can be interpreted as the

average frequency for a healthy fish that both assimilate the required energy and meets metabolic demands.

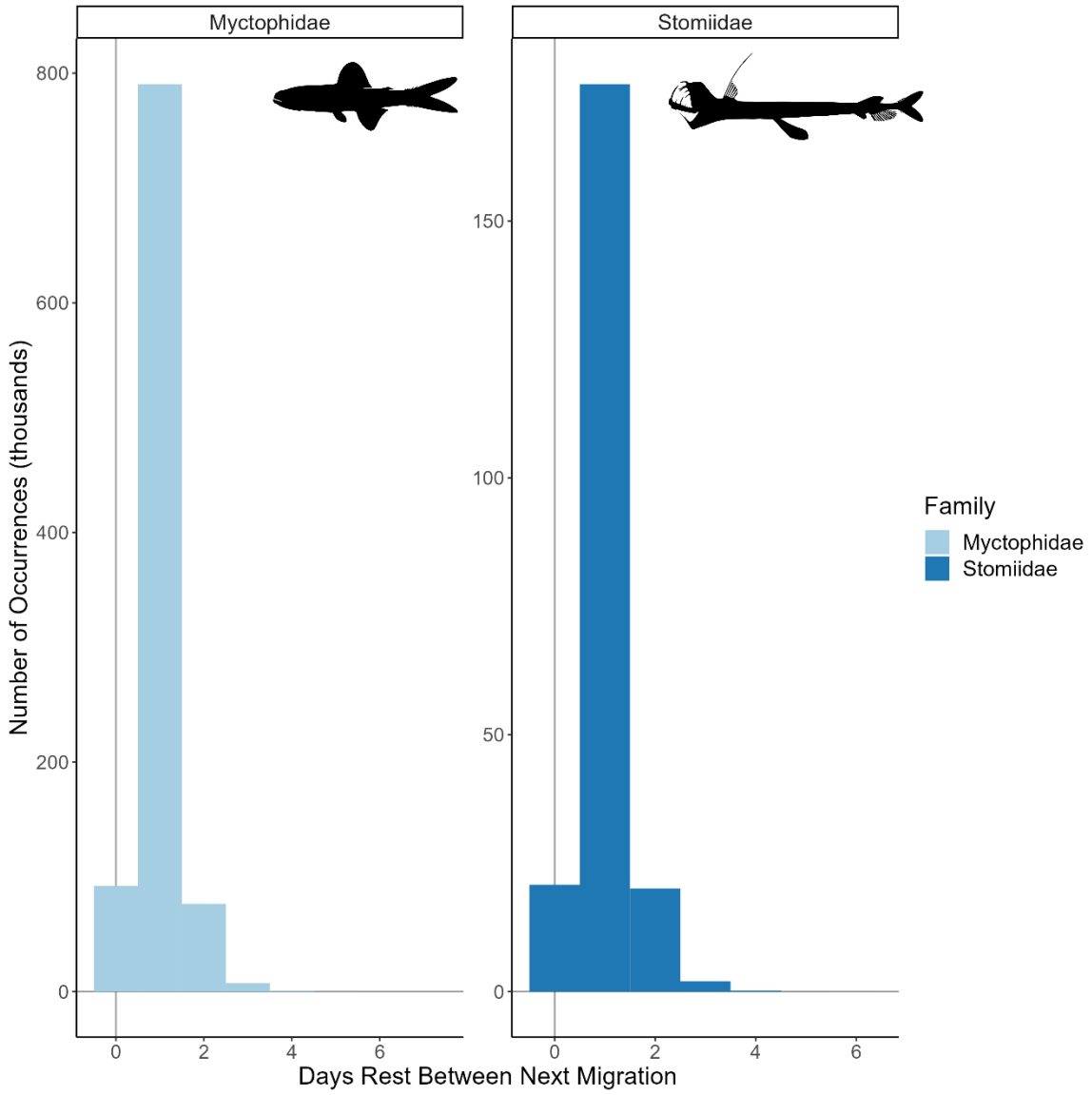

Figure 4. The frequency of days rest in between migrations for all asynchronous vertical migrators (n = 28). The x-axis values represent the maximum values per family. Unaggregated results for all asynchronous vertical migrating species are shown in Figure S2.

Carbon export scenarios

The particulate organic carbon transported across the flux boundary was not different among the three depth scenarios (100, 150, and 200 m). Defecated carbon was added to the water column by vertical migrators at rates of 0.41 (± 0.18), 0.39 (± 0.18), and 0.36 (± 0.18) mg C m^{-2} d^{-1} for the 100-m, 150-m, and 200-m boundary scenarios, respectively, with no signal of seasonality. On average, the contribution of defecated C to the particulate organic carbon in the water column ranged from 4.0–8.6%, with a maximum daily contribution of 25.3%. Excretory flux as calcium carbonate for the assemblage amounted to less than 0.1% of the total particulate organic carbon contribution in all scenarios. Carbon lost from the assemblage through mortality contributed just 0.05 (±0.02) mg C m^{-2} d^{-1} but is associated with a considerable amount of uncertainty that is caused by the stochastic nature of individual mortality (Figure 5). Carbon was respired at rates of 0.57 (± 0.31), 0.65 (± 0.30), and 0.63 (± 0.30) mg C m^{-2} d^{-1} for the 100-m, 150-m, and 200-m scenarios, respectively. However, just 0.3 (53%), 0.49 (75%), and 0.44 (70%) mg C m^{-2} was respired below the flux boundaries, and thus considered transported. The mean respiratory fluxes relative to the water column particulate organic carbon ranged from 7.3–15.2%, and the maximum was 45.8%. The respiratory flux contribution to the water column was 1.7 times the fecal contribution for the vertically migrating fish assemblage (Figure 5). Considering all bioenergetic processes, 61% of ingested carbon was lost from the assemblage, while 39% was retained (Figure 5). The total contribution to the particulate organic carbon pool by mesopelagic fishes in the Gulf of Mexico ranged from 11.4–23.9%, with the possibility to be 71.1% at the upper limit of uncertainty.

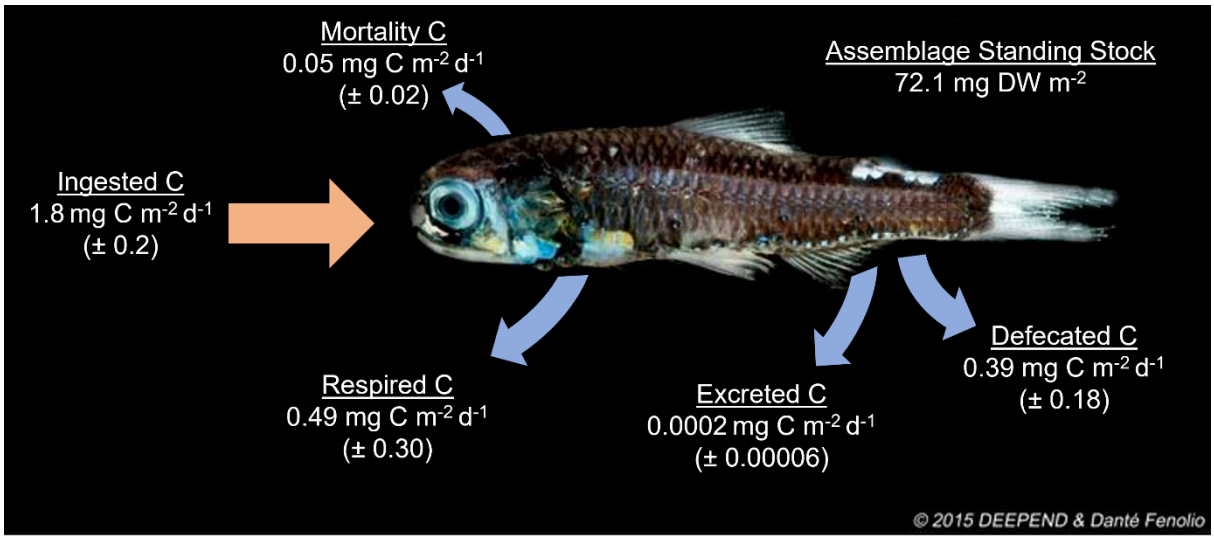

Figure 5. The carbon budget for the vertically migrating assemblage. Flows are represented by arrows, with the orange arrow portraying carbon entering the assemblage and blue arrows showing carbon exported by the assemblage. Values correspond to the 150-m flux boundary scenario and the contribution of diel vertical migrators only. The *Diaphus mollis* image is courtesy of Danté Fenolio and the DEEPEND Consortium.

The total carbon flux for the mesopelagic assemblage was 0.70 (± 0.54), 0.88 (± 0.74), and 0.80 (± 0.64) mg C m^{-2} d^{-1} for the 100-m, 150-m, and 200-m scenarios, respectively (Table 2). The family Myctophidae accounted for at least 53% of the assemblage carbon flux in all three scenarios (Table 2). Two myctophids, *Lepidophanes guentheri* and *Lampanyctus alatus* each contributed greater than 10% of the total carbon flux in the 150-m flux scenario. The 30 most abundant species accounted for 41.5% of the assemblage carbon export. Although the Gonostomatidae accounted for greater than 60% of the relative assemblage abundance, this family contributed just 8.2%, 6.1%, and 6.3% of the carbon flux in the 100-m, 150-m, and 200-m scenarios (Table 2). The gonostomatid contribution was largely *Sigmops elongatus*, which accounted for 0.050 (±0.092), 0.045 (± 0.084), and 0.042 (± 0.078) mg C m^{-2} d^{-1} in the 100-m, 150-m, and 200-m scenarios. Despite occupying just 1.7% of the assemblage abundance, stomiids accounted for greater than 12% of the total carbon flux by the assemblage in all scenarios (Table 2). Individually, the most abundant species in the ecosystem made a large

373 proportion of the carbon flux, but the assemblage diversity and the large body size of rare species
374 also elevated the assemblage-based carbon export value.
375

Table 2. The carbon transport of vertically migrating mesopelagic families is ordered by the sample size of vertical migrators only. Assemblage values are in bold. Flux values are in the units mg C m^{-2} d^{-1} (mean ± sd). Percent values are the proportion of the total assemblage carbon flux for each scenario

	100 m		150 m		200 m	
Family	**Value**	**%**	**Value**	**%**	**Value**	**%**
Assemblage	**$7.1 \times 10^{-1} \pm 5.4 \times 10^{-1}$**	**-**	**$8.8 \times 10^{-1} \pm 7.4 \times 10^{-1}$**	**-**	**$8.0 \times 10^{-1} \pm 6.4 \times 10^{-1}$**	**-**
Myctophidae	$3.7 \times 10^{-1} \pm 2.7 \times 10^{-1}$	53.1%	$5.4 \times 10^{-1} \pm 4.5 \times 10^{-1}$	61.6%	$5.0 \times 10^{-1} \pm 3.7 \times 10^{-1}$	62.2%
Stomiidae	$1.6 \times 10^{-1} \pm 1.1 \times 10^{-1}$	22.7%	$1.4 \times 10^{-1} \pm 1.1 \times 10^{-1}$	15.9%	$1.3 \times 10^{-1} \pm 1.0 \times 10^{-1}$	15.7%
Gonostomatidae	$5.8 \times 10^{-2} \pm 9.4 \times 10^{-2}$	8.2%	$5.3 \times 10^{-2} \pm 8.5 \times 10^{-2}$	6.1%	$5.0 \times 10^{-2} \pm 7.9 \times 10^{-2}$	6.3%
Sternoptychidae	$1.0 \times 10^{-2} \pm 1.4 \times 10^{-2}$	1.4%	$4.4 \times 10^{-2} \pm 6.0 \times 10^{-2}$	5.1%	$3.4 \times 10^{-2} \pm 4.4 \times 10^{-2}$	4.2%
Melamphaidae	$1.5 \times 10^{-2} \pm 5.7 \times 10^{-3}$	2.2%	$3.0 \times 10^{-2} \pm 7.8 \times 10^{-3}$	3.5%	$3.1 \times 10^{-2} \pm 9.3 \times 10^{-3}$	3.9%
Scopelarchidae	$1.9 \times 10^{-2} \pm 1.3 \times 10^{-2}$	2.6%	$1.5 \times 10^{-2} \pm 8.5 \times 10^{-3}$	1.7%	$1.4 \times 10^{-2} \pm 9.5 \times 10^{-3}$	1.7%
Paralepididae	$1.5 \times 10^{-2} \pm 4.5 \times 10^{-3}$	2.1%	$1.3 \times 10^{-2} \pm 2.9 \times 10^{-3}$	1.5%	$1.4 \times 10^{-2} \pm 2.9 \times 10^{-3}$	1.7%
Phosichthyidae	$1.3 \times 10^{-2} \pm 4.7 \times 10^{-3}$	1.8%	$8.5 \times 10^{-3} \pm 5.2 \times 10^{-3}$	1.0%	$6.4 \times 10^{-3} \pm 3.9 \times 10^{-3}$	0.8%
Chiasmodontidae	$1.1 \times 10^{-2} \pm 1.2 \times 10^{-2}$	1.6%	$8.6 \times 10^{-3} \pm 5.5 \times 10^{-3}$	1.0%	$6.2 \times 10^{-3} \pm 7.6 \times 10^{-3}$	0.8%
Notosudidae	$7.8 \times 10^{-3} \pm 3.0 \times 10^{-3}$	1.1%	$7.5 \times 10^{-3} \pm 3.1 \times 10^{-3}$	0.9%	$7.0 \times 10^{-3} \pm 2.4 \times 10^{-3}$	0.9%
Bregmacerotidae	$9.4 \times 10^{-3} \pm 5.0 \times 10^{-3}$	1.3%	$6.9 \times 10^{-3} \pm 4.4 \times 10^{-3}$	0.8%	$7.2 \times 10^{-3} \pm 3.7 \times 10^{-3}$	0.9%
Percophidae	$8.9 \times 10^{-3} \pm 1.7 \times 10^{-3}$	1.3%	$6.9 \times 10^{-3} \pm 1.3 \times 10^{-3}$	0.8%	$5.2 \times 10^{-3} \pm 1.3 \times 10^{-3}$	0.6%
Evermannellidae	$1.7 \times 10^{-3} \pm 6.6 \times 10^{-4}$	0.2%	$1.5 \times 10^{-3} \pm 7.8 \times 10^{-4}$	0.2%	$1.3 \times 10^{-3} \pm 4.7 \times 10^{-4}$	0.2%
Gempylidae	$7.2 \times 10^{-4} \pm 4.2 \times 10^{-4}$	0.1%	$6.9 \times 10^{-4} \pm 5.8 \times 10^{-4}$	0.1%	$5.3 \times 10^{-4} \pm 4.1 \times 10^{-4}$	0.1%
Trichiuridae	$1.3 \times 10^{-3} \pm 1.1 \times 10^{-4}$	0.2%	$1.1 \times 10^{-3} \pm 9.7 \times 10^{-5}$	0.1%	$9.2 \times 10^{-4} \pm 9.6 \times 10^{-5}$	0.1%
Howellidae	$1.6 \times 10^{-6} \pm 1.5 \times 10^{-7}$	<0.1%	$1.6 \times 10^{-6} \pm 1.3 \times 10^{-7}$	<0.1%	$1.5 \times 10^{-6} \pm 1.3 \times 10^{-7}$	<0.1%

Sensitivity analysis

A sensitivity analysis revealed the parameters that most influenced the model (Table 3). Temperature changes resulted in a 51% increase in particulate organic carbon flux contribution when increased by 20% and a 34% reduction when the temperature was decreased by 20%. Activity rate parameters (e.g., AMR, and migration time) changed the carbon export value by 15% (Table 5). Interestingly, the model was similarly sensitive to ingestion coefficients and prey quality (for a crustacean eater). Adjustments to the predation success parameters did not influence the model results by more than 3% in any scenario (Table 3), suggesting that a 10% deviation to predation success does not significantly impact carbon flux rates. The model's sensitivity is related to the use of a metabolic rate equation to regulate all other bioenergetic processes in the model.

Table 3. Results in terms of the particulate organic carbon contribution to the assemblage from a sensitivity analysis of a 30 mm SL *Lampanyctus alatus* retained at the same depths, longitude, and latitude for 1,000 iterations. Low and High factors are the values multiplied by the default value for that parameter. Values in italics are the actual value used in the scenario, rather than a multiplicative parameter. Ratios were calculated as the simulated value divided by a base scenario (all default parameters)

Parameter	Low Factor	High Factor	Low:Base	High:Base
Active Metabolic Rate	0.8	1.2	0.85	1.15
Caloric Content of Prey	0.8	1.2	0.89	1.17
Ingestion Coefficient	0.8	1.2	1.23	0.85
Migration Time	*3*	*5*	0.85	1.15
Mortality	0.8	1.2	0.96	1.05
Predation Success Day	*0*	*0.1*	1.00	0.99
Predation Success Night	*0.8*	*1*	0.97	1.03
Respiratory Quotient	*0.7*	*1*	0.98	1.01
Standard Metabolic Rate	0.8	1.2	0.95	1.05
Temperature	0.8	1.2	0.66	1.51

Discussion

The development of a trait-based bioenergetic model for individual mesopelagic fishes advances understanding of open carbon export by incorporating species-specific characteristics and stochasticity into the equation. Including species-specific differences in diel depth occupancy and vertical migratory behavior along with randomness within depth ranges influences the metabolic rate estimates in the *RMR* equation that was used (Ikeda 2016). Similarly, differences in prey quality affect the amount of carbon an individual ingests per feeding period, which is a more realistic estimation than assuming all species ingest the same prey taxa. The uncertainty in bioenergetic rates estimated by this model is greater than other carbon export models that use a similar algorithm (Hidaka et al. 2001; Davison et al. 2013). However, this decrease in precision is partially caused by individual variability, differences in diet among species, diel depth differences, diel vertical migratory behavior, which are all present factors in oceanic ecosystems. Individual variability and ontogenic changes in depth occupancy, migratory behavior, and diet are not fully resolved within the assemblage, but do exist (Lancraft

et al. 1988; Hopkins and Gartner 1992; Christiansen et al. 2021), indicating that this modeling framework could be advanced pending a sufficient amount of life history information. To understand bioenergetic rates at a population, community, or global scale, it is imperative to understand the variation caused by individuals within a species to calculate the magnitude of this variation at a higher order.

Bioenergetic rates

The use of metabolic rates to estimate ingestion rates produces values comparable to empirical and model estimates. In this study, myctophid daily rations range from 0.3–8.5%, with a geometric mean of 3.0%. In other regions, myctophid rations range from 0.2–4.4% bodyweight consumed (Pakhomov et al. 1996; Pusch et al. 2004; Tanaka et al. 2013). The myctophid species with rations beyond the literature values are synchronous migrators that ascend above the thermocline each night (e.g., *Myctophum affine;* Hopkins and Gartner 1992), experiencing the most extreme metabolic requirements. Stomiids in the Gulf of Mexico have average instantaneous rations that range from 2.1–7.6, but their maximum rations (largest % bodyweight observed) can be as high as 99% bodyweight (Sutton and Hopkins 1996). In this study, stomiid percent bodyweight consumed per feeding interval ranged from 0.3–3.5% with a geometric mean of 1.9% for all species, suggesting that stomiids likely consume more than is necessary to meet their minimum energetic requirement. Alternatively, this model may underestimate activity rates that would increase their metabolic requirements, and subsequently feeding rations.

Although prey taxa were coarse (e.g., crustacean, fish, cephalopod, gelatinous zooplankton), the type of prey a fish predominantly consumed influenced the percent bodyweight consumed per feeding interval. Gelatinous zooplankton is historically underrepresented in diet studies because of rapid digestion rates and difficulties with taxonomic identification, creating the “jelly

web" (Robison 2004). These soft-bodied taxa may represent a greater proportion of diets than are able to be incorporated here, and our results suggest that the inclusion of lower quality prey increases rations. Essentially, the consumption of lesser quality prey (lower caloric content per g of prey) leads to a fish having to consume more biomass to acquire a sufficient number of resources for their energetic demand. The modeled rations align with empirical daily ration estimates that are typically derived from stomach fullness values and gut evacuation rates, indicating that these methods are comparable to simulations developed from metabolic theory.

Asynchronous vertical migration

The periodicity of asynchronous vertical migration is an important carbon budget parameter, as mesopelagic fishes will only actively transport carbon if they ascend beyond the flux boundary. In this model, the process of asynchronous vertical migration was driven by the energy reserves an individual fish was currently storing. Energy assimilation and usage were both functions of body mass, and therefore all species had a similar asynchronous migration periodicity. On 81% of occasions, fishes took one day of rest before migrating again. Davison et al. (2013) used the difference between "shallow" and "deep" micronekton trawls to estimate that ~50% of the vertically migrating mesopelagic biomass migrates each night in the California current region, which could be interpreted as a migration periodicity of one day's rest per individual, similar to the results of this model. This model indicates that fishes may migrate on successive nights (10% likelihood), but it is possible that they rest for a full week. Sutton and Hopkins (1996) estimated that stomiids in the Gulf of Mexico only feed once every eight days based on their instantaneous ration and gastric evacuation rates. Hypothetically, stomiids may have a larger ration (Sutton and Hopkins 1996) and lower activity rates (i.e., sit-and-wait predation strategy; Feagans-Bartow and Sutton 2014) than modeled in this study. The realistic

asynchronous migration periodicity is reliant on enigmatic, species-specific activity rates, which could not be modeled in this study. However, assuming that the entirety of a population migrates each night, instead of a proportion, may inflate nutrient flux and other bioenergetic rate estimates.

Flux boundaries in carbon export models

Adjusting the flux boundary did not reveal differences in carbon export rates within species, which were retained at the assemblage scale. However, in the 150-m and 200-m flux boundary scenarios, greater than 70% of the respired carbon occurred below the flux boundary, as opposed to 53% in the 100-m flux boundary. Although counterintuitive, the shallowest fishes in the water column experience the warmest temperatures and have the highest respiration rates, relative to deeper-dwelling fishes. Species-specific differences among flux boundary scenarios were a product of the depth ranges of organisms (e.g., some fishes only migrate to 175 m at night; Hopkins and Gartner 1992), which is reflected at the assemblage scale. Therefore, vertically migrating fishes ascending above the 100-m depth boundary (i.e., fishes considered in the 100-m flux boundary scenario) may respire a lesser proportion of carbon below the flux boundary when compared to the 150-m and 200-m flux boundary scenarios. The depth a fish ascends to during diel vertical migration is primarily a light-driven process (Boswell et al. 2020), but other factors can influence individual fish behavior as well, such as the presence of predators and fish size (Urmy and Benoit-Bird 2021), indicating that the inclusion of a singular nighttime depth for all mesopelagic fishes will introduce uncalculated error in bioenergetic models. Refinement of depth distribution information and increased understanding of flux boundary depths will enhance fish-mediated carbon export modeling efforts in the open ocean.

Comparison to other carbon export studies

Carbon export by mesopelagic fishes contributes significantly to the carbon transported into the mesopelagic zone, particularly in oligotrophic regions. The fecal contribution to the total particulate organic carbon standing stock in the water column ranged from 0.04–25.3%. A previous fecal carbon contribution estimate for mesopelagic fishes in the eastern Gulf of Mexico was 0.5–0.9 mg C m^{-2} d^{-1} (Hopkins et al. 1996). The fecal carbon flux rate in this model ranged from 0.18–0.57 mg C m^{-2} d^{-1}. Although the upper confidence levels of all scenarios do enter the range of the previous estimate, the mean values are below 0.5. Any difference in carbon export is most likely explained by the previous standing stock estimate of 296 mg DW m^{-2}, 4.1 times greater than the current modeled standing stock estimate. The difference in standing stock values may be attributed to 1) the difference between the biomass estimated from the direct weighing of trawl catches and length-weight regression estimates based on measuring trawl catches and 2) a decline in mesopelagic fish biomass in the Gulf of Mexico that has occurred since 2011 (Sutton et al. submitted). Although model uncertainty and a lack of flux boundary depth confirmation remove our ability to determine if the fecal carbon contribution has declined, further exploration is required given the mean and lower confidence level limits to all scenarios.

The fish-mediated carbon flux estimates for the northern Gulf of Mexico are reasonable compared to other localities. The fish-mediated carbon export rates in other oligotrophic, open-ocean regions range from 0.04 mg C m^{-2} d^{-1} near the Mid-Atlantic Ridge (Hudson et al. 2014) to 11.5 mg C m^{-2} d^{-1} in the tropical Atlantic Ocean (Hernández-León et al. 2019b). In the oceanic Gulf of Mexico, the vertically migrating fish assemblage contributed between 0.14–0.72 mg C m^{-2} d^{-1}. Respiratory flux ranged from 0.03–45.8% POC, depending on the scenario. Estimates for respiratory flux range from 1.2–10.4% POC in the Canary Islands (Ariza et al. 2015), 12–32%

POC in the tropical Atlantic Ocean Hernández-León et al. (2019b), and 1–47% POC in the Scotia Sea. There is a wide range in the results of carbon export models due to the differences in the use of bioenergetic rate equations, fish communities, and environmental conditions (i.e., water temperature). Consistency among these modeling objectives will be critical to estimate the contribution of mesopelagic fishes to the global carbon budget, but the regional mesopelagic community and biogeochemical differences may also influence local carbon export rates.

Acknowledgements

This paper is a result of research funded by the National Oceanic and Atmospheric Administration's RESTORE Science Program under award NA19NOS4510193 to Nova Southeastern University and The Gulf of Mexico Research Initiative. This is publication #1433 from the Institute of Environment at Florida International University. The authors are grateful to Kevin Boswell for comments on the model framework.

Data Availability Statement

Data are publicly available through the Gulf of Mexico Research Initiative Information & Data Cooperative (GRIIDC) at https://data.gulfresearchinitiative.org (doi: 10.7266/N7VX0DK2; 10.7266/N70P0X3T; 10.7266/N7XP7385; 10.7266/N7902234; 10.7266/n7-ac8e-0240).

Literature Cited

Angel, M. V. 1993. Biodiversity of the pelagic ocean. Conserv. Biol. **7**: 760–772. doi:10.1046/j.1523-1739.1993.740760.x

Archibald, K. M., D. A. Siegel, and S. C. Doney. 2019. Modeling the impact of zooplankton diel vertical migration on the carbon export flux of the biological pump. Global Biogeochem. Cycles **33**: 181–199. doi:10.1029/2018GB005983

Ariza, A., J. C. Garijo, J. M. Landeira, F. Bordes, and S. Hernández-León. 2015. Migrant

biomass and respiratory carbon flux by zooplankton and micronekton in the subtropical northeast Atlantic Ocean (Canary Islands). Prog. Oceanogr. **134**: 330–342. doi:10.1016/j.pocean.2015.03.003

Bianchi, D., and K. A. S. Mislan. 2016. Global patterns of diel vertical migration times and velocities from acoustic data. Limnol. Oceanogr. **61**: 353–364. doi:10.1002/lno.10219

Bishop, R. E., and J. J. Torres. 2001. Leptocephalus energetics: assembly of the energetics equation. Mar. Biol. **138**: 1093–1098. doi:https://doi.org/10.1007/s002270100541

Bos, R. P., T. T. Sutton, and T. M. Frank. 2021. State of satiation partially regulates the dynamics of vertical migration. Front. Mar. Sci. **8**: 1–11. doi:10.3389/fmars.2021.607228

Boswell, K. M., M. D'Elia, M. W. Johnston, J. A. Mohan, J. D. Warren, R. J. D. Wells, and T. T. Sutton. 2020. Oceanographic structure and light levels drive patterns of sound scattering layers in a low-latitude oceanic system. Front. Mar. Sci. **7**: 51. doi:10.3389/fmars.2020.00051

Brett, J., and T. Groves. 1979. Physiological energetics: volume VIII, bioenergetics and growth, p. 280–352. *In* W.S. Hoar, D.J. Randall, and J.R. Brett [eds.], Fish Physiology. Academic Press.

Buesseler, K. O., P. W. Boyd, E. E. Black, and D. A. Siegel. 2020. Metrics that matter for assessing the ocean biological carbon pump. Proc. Natl. Acad. Sci. **117**: 9679–9687. doi:10.1073/pnas.1918114117/-/DCSupplemental

Childress, J. J., and G. N. Somero. 1979. Depth-related enzymic activities in muscle, brain and heart of deep-living pelagic marine teleosts. Mar. Biol. **52**: 273–283. doi:https://doi.org/10.1007/BF00398141

Choy, C. A., S. H. D. Haddock, and B. H. Robison. 2017. Deep pelagic food web structure as

549 revealed by in situ feeding observations. Proc. R. Soc. B **284**: 20172116.
550 doi:10.1098/rspb.2017.2116
551 Christiansen, S., T. A. Klevjer, A. Røstad, D. L. Aksnes, and S. Kaartvedt. 2021. Flexible
552 behaviour in a mesopelagic fish (*Maurolicus muelleri*). ICES J. Mar. Sci.
553 doi:10.1093/icesjms/fsab075
554 Clarke, T. M. 1978. Dial feeding patterns of 16 species of mesopelagic fishes from Hawaiian
555 waters. Fish. Bull. **76**: 495–513.
556 Cook, A. B., A. M. Bernard, K. M. Boswell, and others. 2020. A multidisciplinary approach to
557 investigate deep-pelagic ecosystem dynamics in the Gulf of Mexico following Deepwater
558 Horizon. Front. Mar. Sci. **7**: 1–14. doi:10.3389/fmars.2020.548880
559 Davison, P. C. C., D. M. M. Checkley, J. A. A. Koslow, and J. Barlow. 2013. Carbon export
560 mediated by mesopelagic fishes in the northeast Pacific Ocean. Prog. Oceanogr. **116**: 14–
561 30. doi:10.1016/J.POCEAN.2013.05.013
562 Ducklow, H. W., D. K. Steinberg, and K. O. Buesseler. 2001. Upper ocean carbon export and the
563 biological pump. Oceanography **14**: 50–58.
564 Eppley, R. W. 1972. Temperature and phytoplankton growth in the sea. Fish. Bull. **70**: 1063–
565 1085.
566 Feagans-Bartow, J. N., and T. T. Sutton. 2014. Ecology of the oceanic rim: pelagic eels as key
567 ecosystem components. Mar. Ecol. Prog. Ser. **502**: 257–266. doi:10.3354/meps10707
568 Gartner Jr, J. V., T. L. Hopkins, R. C. Baird, and D. M. Milliken. 1987. The lanternfishes (Pices:
569 Myctophidae) of the Eastern Gulf of Mexico. Fish. Bull. **35**: 81–98.
570 Gibbs, A., and G. N. Somero. 1989. Pressure adaptation of Na+/K+-ATPase in gills of marine
571 teleosts. J. Exp. Biol. **143**: 475–492. doi:10.1242/jeb.143.1.475

572 Gillooly, J., J. Brown, G. West, and others. 2001. Effects of size and temperature on metabolic
573 rate. Science (80-.). **293**: 2248–2251. doi:10.1126/science.1061967
574 Haddock, S. H. D. 2004. A golden age of gelata: Past and future research on planktonic
575 ctenophores and cnidarians. Hydrobiologia **530**–**531**: 549–556. doi:10.1007/s10750-004-
576 2653-9
577 Haedrich, R. L. 1996. Deep-water fishes: Evolution and adaptation in the earth's largest living
578 spaces. J. Fish Biol. **49**: 40–53. doi:10.1111/j.1095-8649.1996.tb06066.x
579 Hernández-León, S., S. Calles, and M. Luz Fernández De Puelles. 2019a. The estimation of
580 metabolism in the mesopelagic zone: Disentangling deep-sea zooplankton respiration. Prog.
581 Oceanogr. **178**: 102163. doi:10.1016/j.pocean.2019.102163
582 Hernández-León, S., M. P. Olivar, M. L. Fernández de Puelles, A. Bode, A. Castellón, C. López-
583 Pérez, V. M. Tuset, and J. I. González-Gordillo. 2019b. Zooplankton and micronekton
584 active Flux across the tropical and subtropical Atlantic Ocean. Front. Mar. Sci. **6**: 1–20.
585 doi:10.3389/fmars.2019.00535
586 Hidaka, K., K. Kawaguchi, M. Murakami, and M. Takahashi. 2001. Downward transport of
587 organic carbon by diel migratory micronekton in the western equatorial pacific: Its
588 quantitative and qualitative importance. Deep. Res. Part I Oceanogr. Res. Pap. **48**: 1923–
589 1939. doi:10.1016/S0967-0637(01)00003-6
590 Hopkins, T. L., and J. V Gartner. 1992. Resource-partitioning and predation impact of a low-
591 latitude myctophid community. Mar. Biol. **114**: 185–197. doi:10.1007/BF00349518
592 Hopkins, T. L., T. T. Sutton, and T. M. Lancraft. 1996. The trophic structure and predation
593 impact of a low latitude midwater fish assemblage. Prog. Oceanogr. **38**: 205–239.
594 Hudson, J. M., D. K. Steinberg, T. T. Sutton, J. E. Graves, and R. J. Latour. 2014. Myctophid

595 feeding ecology and carbon transport along the northern Mid-Atlantic Ridge. Deep. Res.
596 Part I Oceanogr. Res. Pap. **93**: 104–116. doi:10.1016/j.dsr.2014.07.002
597 Ikeda, T. 2016. Routine metabolic rates of pelagic marine fishes and cephalopods as a function
598 of body mass, habitat temperature and habitat depth. J. Exp. Mar. Bio. Ecol. **480**: 74–86.
599 doi:10.1016/j.jembe.2016.03.012
600 Irigoien, X., T. A. Klevjer, A. Røstad, and others. 2014. Large mesopelagic fishes biomass and
601 trophic efficiency in the open ocean. Nat. Commun. **5**: 3271. doi:10.1038/ncomms4271
602 Johnston, M. W., and A. M. Bernard. 2017. A bank divided: quantifying a spatial and temporal
603 connectivity break between the Campeche Bank and the northeastern Gulf of Mexico. Mar.
604 Biol. **164**: 1–15. doi:10.1007/s00227-016-3038-0
605 Johnston, M. W., R. J. Milligan, C. G. Easson, S. deRada, D. C. English, B. Penta, and T. T.
606 Sutton. 2019. An empirically validated method for characterizing pelagic habitats in the
607 Gulf of Mexico using ocean model data. Limnol. Oceanogr. Methods **17**: lom3.10319.
608 doi:10.1002/lom3.10319
609 Judkins, D. C. 2014. Geographical distribution of pelagic decapod shrimp in the Atlantic Ocean.
610 Zootaxa **3895**: 301–345. doi:10.11646/zootaxa.3895.3.1
611 Jusup, M., T. Klanjscek, H. Matsuda, and S. A. L. M. Kooijman. 2011. A full lifecycle
612 bioenergetic model for bluefin tuna. PLoS One **6**: e21903.
613 doi:10.1371/journal.pone.0021903
614 Kooijman, S. A. L. M. 2010. Dynamic Energy Budget theory for metabolic organisation :
615 Summary of concepts of the third edition, Cambridge University Press.
616 Koslow, J. A., R. J. Kloser, and A. Williams. 1997. Pelagic biomass and community structure
617 over the mid-continental slope off southeastern Australia based upon acoustic and midwater

618 trawl sampling. Mar. Ecol. Prog. Ser. **146**: 21–35. doi:10.3354/meps146021
619 Lancraft, T., T. L. Hopkins, and J. J. Torres. 1988. Aspects of the ecology of the mesopelagic
620 fish *Gonostoma elongatum* (Gonostomatidae, Stomnformes) in the eastern Gulf of Mexico.
621 Mar. Ecol. Prog. Ser. **49**: 27–40. doi:10.3354/meps049027
622 Lomas, M. W., D. K. Steinberg, T. Dickey, C. Carlson, N. Nelson, R. Condon, and N. Bates.
623 2010. Increased ocean carbon export in the Sargasso Sea linked to climate variability is
624 countered by its enhanced mesopelagic attenuation. Biogeosciences **7**: 57–70.
625 doi:10.5194/bg-7-57-2010
626 Pakhomov, E. A., R. Perissinotto, and C. D. McQuaid. 1996. Prey composition and daily rations
627 of myctophid fishes in the Southern Ocean. Mar. Ecol. Prog. Ser. **134**: 1–14.
628 doi:10.3354/meps134001
629 Pearcy, W. G., H. V Lorz, and W. Peterson. 1979. Comparison of the Feeding Habits of
630 Migratory and Non-Migratory *Stenobrachius leucopsarus* (Myctophidae). Mar. Biol. **51**: 1–
631 8.
632 Pearre, S. 2003. Eat and run? The hunger/satiation hypothesis in vertical migration: History,
633 evidence and consequences. Biol. Rev. Camb. Philos. Soc. **78**: 1–79.
634 doi:10.1017/S146479310200595X
635 Proud, R., N. O. Handegard, R. J. Kloser, M. J. Cox, A. S. Brierley, and D. Demer. 2019. From
636 siphonophores to deep scattering layers: Uncertainty ranges for the estimation of global
637 mesopelagic fish biomass. ICES J. Mar. Sci. **76**: 718–733. doi:10.1093/icesjms/fsy037
638 Pusch, C., P. A. Hulley, and K. H. Kock. 2004. Community structure and feeding ecology of
639 mesopelagic fishes in the slope waters of King George Island (South Shetland Islands,
640 Antarctica). Deep. Res. Part I Oceanogr. Res. Pap. **51**: 1685–1708.

641 doi:10.1016/j.dsr.2004.06.008
642 Radchenko, V. I. 2007. Mesopelagic fish community supplies “Biological Pump.” Raffles Bull.
643 Zool. **14**: 265–271. doi:https://doi.org/10.1038/274362a0
644 Robison, B. H. 2004. Deep pelagic biology. J. Exp. Mar. Bio. Ecol. **300**: 253–272.
645 doi:10.1016/j.jembe.2004.01.012
646 Robison, B. H., and T. G. Bailey. 1981. Sinking rates and dissolution of midwater fish fecal
647 matter. Mar. Biol. **65**: 135–142. doi:10.1007/BF00397077
648 Saba, G. K., A. B. Burd, J. P. Dunne, and others. 2021. Toward a better understanding of fish-
649 based contribution to ocean carbon flux. Limnol. Oceanogr. 1–26. doi:10.1002/lno.11709
650 Sauzède, R., J. E. Johnson, H. Claustre, G. Camps-Valls, and A. B. Ruescas. 2020. Estimation of
651 oceanic particulate organic carbon with machine learning. ISPRS Ann. Photogramm.
652 Remote Sens. Spat. Inf. Sci. **2**: 949–956. doi:10.5194/isprs-annals-V-2-2020-949-2020
653 Stickney, D. G., and J. J. Torres. 1989. Proximate composition and energy content of
654 mesopelagic fishes from the eastern Gulf of Mexico. Mar. Biol. **103**: 13–24.
655 doi:10.1007/BF00391060
656 Sutton, T. T. 2013. Vertical ecology of the pelagic ocean: classical patterns and new
657 perspectives. J. Fish Biol. **83**: 1508–1527. doi:10.1111/jfb.12263
658 Sutton, T. T., T. Frank, H. Judkins, and I. C. Romero. 2020. As gulf oil extraction goes deeper,
659 who is at risk? community structure, distribution, and connectivity of the deep-pelagic
660 fauna., *In* S. Murawski, C.H. Ainsworth, S. Gilbert, D.J. Hollander, C.B. Paris, M. Schlüter,
661 and D.L. Wetzel [eds.], Scenarios and Responses to Future Deep Oil Spills. Springer.
662 Sutton, T. T., and T. Hopkins. 1996. Trophic ecology of the stomiid (Pisces: Stomiidae) fish
663 assemblage of the eastern Gulf of Mexico: strategies, selectivity and impact of a top

mesopelagic predator group. Mar. Biol. **127**: 179–192. doi:https://doi.org/10.1007/BF00942102

Tanaka, H., C. Sassa, S. Ohshimo, and I. Aoki. 2013. Feeding ecology of two lanternfishes *Diaphus garmani* and *Diaphus chrysorhynchus*. J. Fish Biol. **82**. doi:10.1111/jfb.12051

Urmy, S. S., and K. J. Benoit-Bird. 2021. Fear dynamically structures the ocean's pelagic zone. Curr. Biol. **31**: 1–7. doi:10.1016/j.cub.2021.09.003

Wilson, R. W., F. J. Millero, J. R. Taylor, P. J. Walsh, V. Christensen, S. Jennings, and M. Grosell. 2009. Contribution of fish to the marine inorganic carbon cycle. Science (80-.). **323**: 359–362. doi:10.1016/j.pepi.2008.05.007

Winberg, G. G. 1956. Rate of metabolism and food requirements of fish. Fish. Res. Board Canada **194**: 1–253.

Woodstock, M. S., T. T. Sutton, T. Frank, and Y. Zhang. 2021. An early warning sign: trophic structure changes in the oceanic Gulf of Mexico from 2011–2018. Ecol. Modell. **445**: 109509. doi:10.1016/j.ecolmodel.2021.109509

Yoon, W., S. Kim, and K. Han. 2001. Morphology and sinking velocities of fecal pellets of copepod, molluscan, euphausiid, and salp taxa in the northeastern tropical Atlantic. Mar. Biol. **139**: 923–928. doi:10.1007/s002270100630

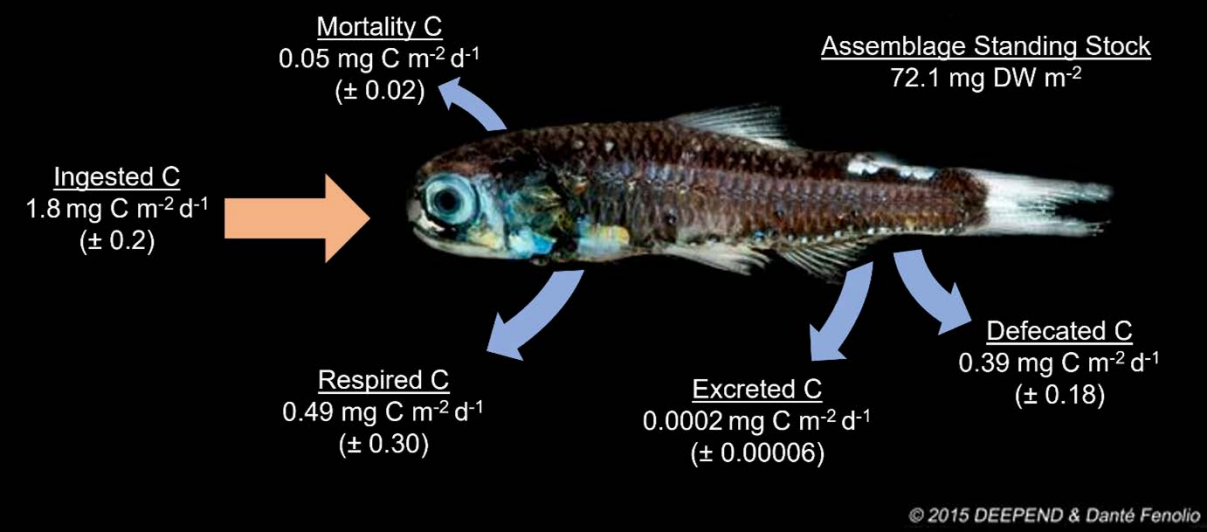
Mortality C
0.05 mg C m-2 d-1
(± 0.02)
Assemblage Standing Stock
72.1 mg DW m-2
Ingested C
1.8 mg C m-2 d-1
(± 0.2)
Respired C
0.49 mg C m-2 d-1
(± 0.30)
Excreted C
0.0002 mg C m-2 d-1
(± 0.00006)
Defecated C
0.39 mg C m-2 d-1
(± 0.18)
© 2015 DEEPEND & Danté Fenolio